Catal Lett (2011) 141:525–530
DOI 10.1007/s10562-010-0482-1

Photoreduction of Carbon Dioxide Over $NaNbO_3$ Nanostructured Photocatalysts

Haifeng Shi · Tingzhi Wang · Jian Chen · Chun Zhu · Jinhua Ye · Zhigang Zou

Received: 3 September 2010 / Accepted: 24 October 2010 / Published online: 6 November 2010

Abstract $NaNbO_3$ had been successfully developed as a new photocatalyst for CO_2 reduction. The catalysts were characterized by X-ray diffraction (XRD), scanning electron microscopy (SEM), and ultraviolet–visible spectroscopy (UV–Vis). The DFT calculations revealed that the top of VB consisted of the hybridized O 2p orbital, while the bottom of CB was constructed by Nb 3d orbital, respectively. In addition, the photocatalytic activities of the $NaNbO_3$ samples for reduction of CO_2 into methanol under UV light irradiation were investigated systematically. Compared with the bulk $NaNbO_3$ prepared by a solid state reaction method, the present $NaNbO_3$ nanowires exhibited a much higher photocatalytic activity for CH_4 production. This is the first example that CO_2 conversion into CH_4 proceeded on the semiconductor nanowire photocatalyst.

Keywords $NaNbO_3$ · Photocatalytic · CO_2 reduction · Nanowires

H. Shi (✉) · T. Wang · J. Chen · C. Zhu
School of Science, Jiangnan University, Wuxi 214122, People's Republic of China
e-mail: shihaifengnju@hotmail.com

H. Shi · Z. Zou
Department of Physics, Eco-Materials and Renewable Energy Research Center (ERERC), Nanjing University, Nanjing 210093, People's Republic of China

H. Shi · J. Ye
Photocatalytic Materials Center (PCMC), National Institute for Materials Science (NIMS) 1-2-1, Sengen, Tsukuba, Ibaraki 305-0047, Japan

1 Introduction

The photocatalytic conversion of carbon oxide (CO_2, green house gas) into valuable chemicals (such as methanol or methane) is of importance in view of preventing the continuous rise in global temperature and providing the alternative fuels [1–4]. In particular, since the first report that the photocatalytic reduction of CO_2 into organic compounds over suspending semiconductor particles in water [1], many efforts have been expanded to develop efficient photocatalysts [5–8]. To date, a large number of reports have focused on the photoreduction of CO_2 over TiO_2-based photocatalysts [9–15]. Recently, some mixed metal oxides such as $FeCaO_4$ [16], $InTaO_4$ [17], and $BiVO_4$ [18] have been developed as photocatalysts for conversion of CO_2 into carbon products. It should be pointed out that the development of new photocatalyst could enhance our understanding of searching for a highly efficient photocatalyst. Thus, developing novel active photocatalysts for CO_2 reduction is still of great interest and urgency.

Environmentally friendly sodium niobate ($NaNbO_3$) is known as a promising lead-free piezoelectric material. More recently, $NaNbO_3$ was developed as an efficient photocatalyst for hydrogen generation [19]. However, to the best of our knowledge, there is no report about the photocatalytic reduction of CO_2 properties of $NaNbO_3$. In addition, the morphology of a photocatalyst strongly affects its photocatalytic activity since the photoreduction reaction occurs on the catalyst surface [20, 21]. Hence, in this study, $NaNbO_3$ with different morphologies was tested as a photocatalyst for photoreduction of carbon dioxide with water under light irradiation. The physical characteristics of samples were examined by the techniques, such as XRD, BET measurement, and UV–vis diffuse reflectance

spectroscopy. The electronic structures of $NaNbO_3$ were investigated using plane-wave based density functional theory calculations.

2 Experimental Section

2.1 Catalyst Synthesis

$NaNbO_3$ bulk powders (SSR) were prepared by a conventional solid-state reaction method according to a previous report [22]. As for the preparation of $NaNbO_3$ nanowires, we first successfully synthesized $Na_2Nb_2O_6{\cdot}H_2O$ nanowires via a facile hydrothermal route and then converted the precursors into $NaNbO_3$ with similar nanostructures by a heating treatment. In a typical case, 1 g of P123 ($EO_{20}PO_{70}EO_{20}$, BASF, USA) was firstly added to 25 ml of distilled water under continuous stirring at 40 °C for 2 h, followed by addition of 5 g of $Nb(OC_2H_5)_5$ (Aldrich, USA). Then NaOH (Wako, Japan) solution (20 mol L^{-1}, 10 ml) was added drop by drop into the above solution. After being stirred for 1 h at 40 °C, the so-obtained suspension was transferred into a Teflon-lined autoclave and thermally treated at 200 °C for 24 h. The so-obtained white precipitate was washed with distilled water and ethanol, and subsequently dried in an oven at 70 °C over night. The so-obtained precursors were heated at 550 °C for 4 h to synthesis the $NaNbO_3$ orthorhombic phase. Platinum-loaded $NaNbO_3$ samples (Pt-$NaNbO_3$) were prepared by a photodeposition method. In a typical case, an aqueous methanol (20 vol.%) solution containing the $NaNbO_3$ powders and hexachloroplatinic acid (0.5% $H_2PtCl_6{\cdot}6H_2O$) was irradiated by a 400 W high-pressure Hg lamp. After 1 h of irradiation, the suspension was filter and dried for 12 h.

2.2 Sample Characterization

The crystal structure of $NaNbO_3$ was determined by an X-ray diffractometer (Utilma III., Japan) with Cu–Kα radiation ($\lambda = 1.54056$ Å) in the 2θ range of 20–80°. The UV–visible diffuse reflectance spectra of the sample were measured in the range of 250–800 nm using an UV–vis spectrophotometer (UV-2550, Shimadzu., Japan) equipped with an integrating sphere attachment. Morphologies of $NaNbO_3$ samples were characterized by a field-emission scanning electron microscope (FE-SEM; JSM-6700, JEOL Co., Japan). The specific surface area was deduced according to Brunauer–Emmett–Teller method by a nitrogen adsorption apparatus (TriStar-3000, Micrometrics., USA) at 77 K.

2.3 Evaluation of Photocatalytic Activity

In this study, we applied the photoreduction of CO_2 into CH_4 to evaluate the property of Pt-$NaNbO_3$ catalyst. Photocatalytic reaction was performed in a Pyrex glass vessel. The $NaNbO_3$ powder sample (0.03 g nanowires; 0.1 g particles) was uniformly and evenly dispersed on the bottom of a small glass cell that was located in the bottom of a Pyrex glass cell, which was connected with a closed system. After replacing the system air into CO_2, 3 ml of H_2O was added into the reactor by a liquid syringe. Then the reactor was stored in the dark condition for 2 h until an adsorption–desorption equilibrium was reached. Finally, the light was irradiated from a 300-W Xe lamp (ILC Technology, CERMAX LX-300). Sample was periodically extracted from the reaction cell to analyze the concentration of CH_4 using a gas chromatograph (GC-14B, Shimadzu., Japan).

2.4 Calculation of Electronic Structure

The ab initio calculations described here were performed with a CASTEP program package based on the density functional theory [23]. A plane wave basis set was used to describe the electronic wave functions with a kinetic energy cutoff of 800 eV. The interactions between ionic cores and valence electrons were represented by ultrasoft pseudopotentials. Exchange–correlation potentials were described by generalized gradient approximations (GGA-PBE). The Brillouin-zone (BZ) integrations of total energy were calculated using the special $5 \times 3 \times 2$ k point generated by the Monkhorst–Pack scheme.

3 Results and Discussion

Figure 1a and b displays the ball-and-stick model and the polyhedron model of $NaNbO_3$, respectively. It was found that $NaNbO_3$ was a typical ABO_3-type pervoskite structure, with an orthorhombic crystal structure (space group, *Pbcm*). The crystal structure of $NaNbO_3$ (Fig. 1b) consisted of NbO_6 octahedron sharing their vertex. As shown in Fig. 1c, It was evident that the $NaNbO_3$ products prepared by a hydrothermal route consisted of straight, smooth, and homogeneous nanowires with a uniform diameter of about 100 nm and length of up to several tens micrometers. The SEM picture of $NaNbO_3$ prepared by a solid-state reaction method (Fig. 1d) revealed that it mainly contained a number of micron-sized particles in addition to some big particles. Figure 2 shows a comparison of the XRD patterns of $NaNbO_3$ samples. All diffraction peaks could be indexed to an orthorhombic structured

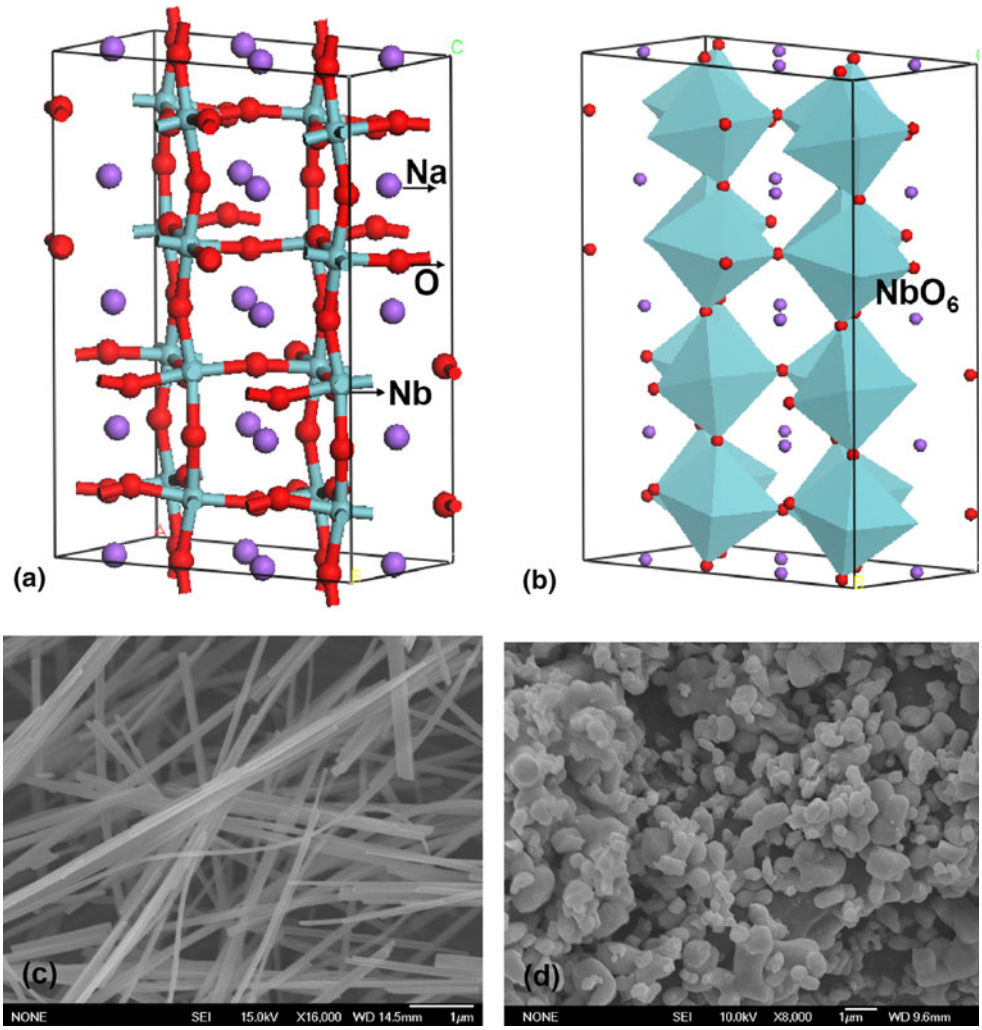

Fig. 1 **a** The ball-and-stick model, **b** the polyhedron model of $NaNbO_3$, **c** SEM image of $NaNbO_3$ prepared by a hydrothermal method, and **d** SEM image of $NaNbO_3$ SSR sample

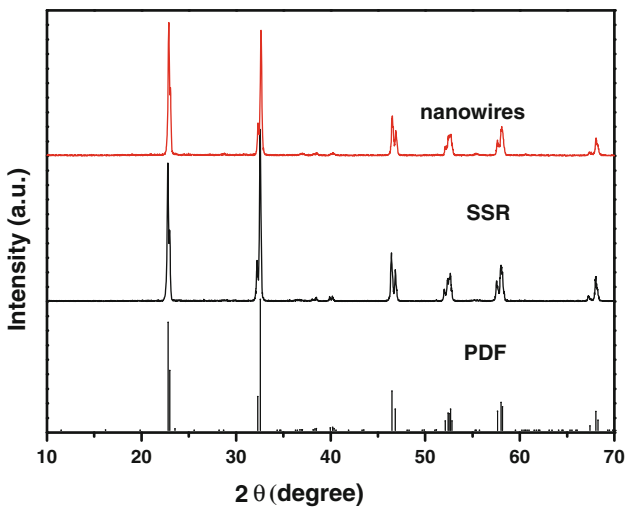

Fig. 2 X-ray diffraction patterns of $NaNbO_3$ samples. As a reference, the standard pattern for $NaNbO_3$ was shown at the *bottom*

$NaNbO_3$, in good agreement with those in the JCPDS Card (No. 01-072-7753).

Figure 3 shows the UV–vis diffuse reflectance spectrum of the sample. The optical band gap E_g of a semiconductor could be deduced according to the following equation

$$(\alpha hv)^n = A\left(hv - E_g\right) \quad (1)$$

where α is the absorption coefficient, hv is the incident photo energy, the value of the index n depends on the electronic transition of the semiconductor ($n_{\text{direct}} = 2$; $n_{\text{indirect}} = 1/2$), A is a proportionality constant related to the material, and E_g is the band gap energy of the semiconductor, respectively. The band gap energy was obtained from the intercept of the tangent line in the plot of $(\alpha hv)^2$ versus energy, and the value was determined to be $\sim$3.4 eV for $NaNbO_3$.

Figure 4 represents the evolved CH_4 concentration over Pt-$NaNbO_3$ catalysts under light irradiation. It was

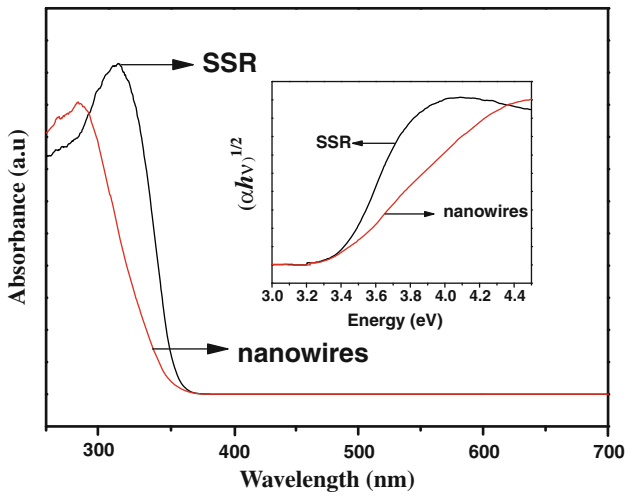

Fig. 3 UV–vis diffuse reflectance spectra of $NaNbO_3$ samples, the *inset* is a plot of $(\alpha hv)^{1/2}$ versus energy (eV) for $NaNbO_3$

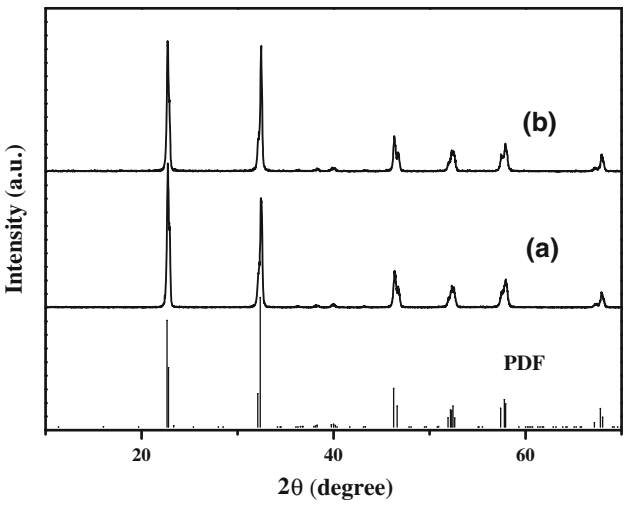

Fig. 5 X-ray diffraction patterns of $NaNbO_3$ nanowires samples before (**a**) and after (**b**) the photocatalytic reaction

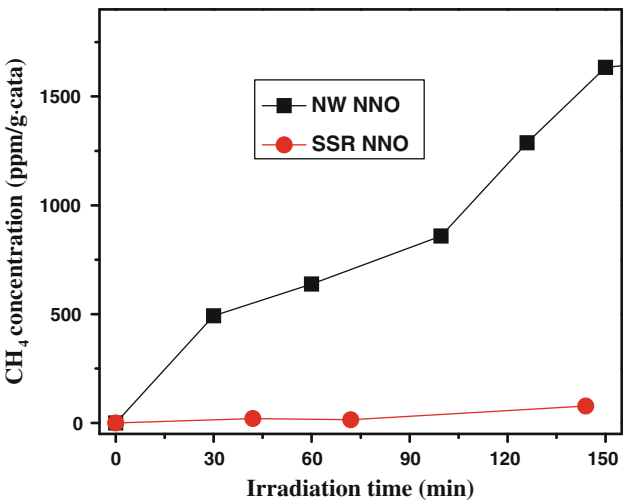

Fig. 4 Photocatalytic methane evolution over Pt-$NaNbO_3$ samples. Reaction conditions: catalyst, 0.1 g SSR $NaNbO_3$ (*SSR NNO*); 0.03 g nanowires $NaNbO_3$ (*NW NNO*)

observed that the CH_4 generated and increased with the prolongation of irradiation time over Pt-$NaNbO_3$ sample, while there was almost no CH_4 to be detected over $NaNbO_3$ under the same reaction conditions. In addition, there was hardly any CH_4 to be observed either under the dark condition or without any catalyst. This implied that the reaction strongly depended on catalyst and light. Namely, the reaction was a photocatalytic reduction process. It was worthwhile to note that the activity of $NaNbO_3$ nanowires is higher than that of $NaNbO_3$ particles, indicating that the $NaNbO_3$ nanowires catalyst has fairly good activity. In order to investigate the photocatalytic repeatability of the catalyst, the photocatalytic reduction of CO_2 over used $NaNbO_3$ nanowires sample was performed again. It was revealed that the photocatalytic activity of used sample was similar to that of the fresh sample.

Figure 5 shows a comparison of the XRD patterns of Pt-$NaNbO_3$ nanowires before and after the photocatalytic reaction. There was no obvious peak change in the XRD patterns of $NaNbO_3$ before and after the photocatalytic reaction, indicating that the phase of Pt-$NaNbO_3$ catalyst was a stable photocatalyst without occurrence of structural degradation during the present photocatalytic reaction process.

The optical properties and the photocatalytic performances of semiconductor photocatalysts are closely related to their electronic structures. We next applied plane-wave based density functional theory calculations (CASTEP program package) to study the band structures of $NaNbO_3$. The DOS (Fig. 6b) displayed that the conduction bands of $NaNbO_3$ are composed of the Nb 3d orbital, while the valence bands are constructed by the hybridized O 2p orbital. The correlation of E and v is known as $v = \Delta_k E(k)/\hbar$, where v is the velocity of electron and E is the energy of electron. If $\Delta_k E(k)$ is large, namely the energy band is dispersive, v will be high. That is, the more dispersive the energy is, the less localized the charge carriers are. As for the present $NaNbO_3$, both calculated CB was abrupt, namely, v of the holes and the electron was high. Hence, the mobility of both charge carriers are high in $NaNbO_3$, leading to promote the photocatalytic activity. On the basis of DFT results, one can see that $NaNbO_3$ has highly mobile charge carriers, which is helpful to carrier transposition in the photocatalysts.

The photocatalytic CO_2 reduction and physical properties of the $NaNbO_3$ photocatalysts were summarized in Table 1. During the first 1.5 h irradiation, the rate of CH_4 generation of $NaNbO_3$ nanowires was as high as 653 ppm h^{-1} g^{-1} in

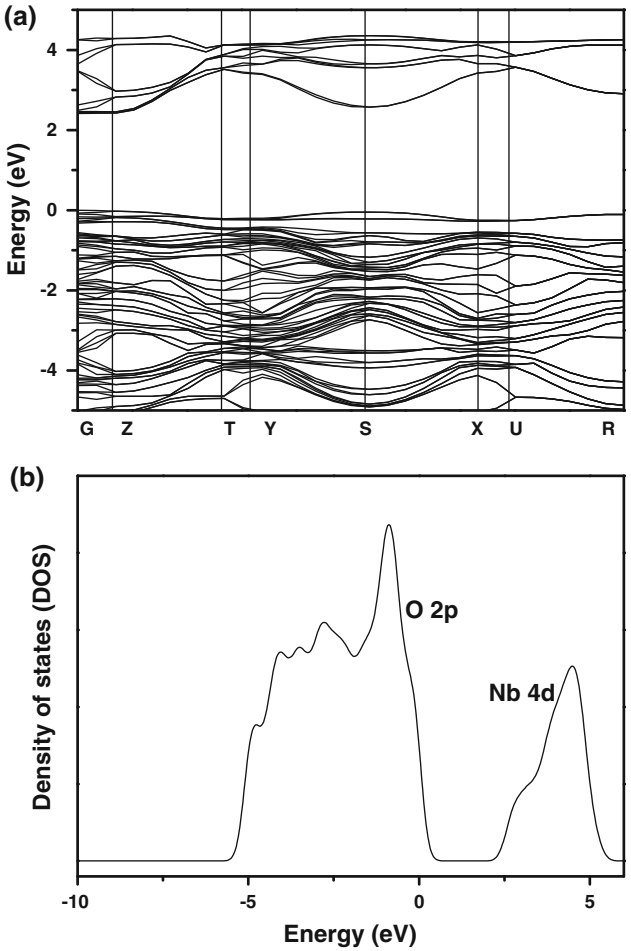

Fig. 6 DFT calculations for $NaNbO_3$, **a** energy band dispersion, and **b** density of states (*DOS*)

Table 1 Photocatalytic activities and physical properties of $NaNbO_3$ photocatalysts

Sample (morphology)	Surface area (m^2 g^{-1})	Rate of CH_4 evolution ppm/(h g)
$NaNbO_3$ (nanowire)	12.0	653
$NaNbO_3$ (bulk)	1.4	32

contrast to that of $NaNbO_3$ particle (22 ppm h^{-1} g^{-1}). Namely, the nanowires structured photocatalyst notably enhanced the photocatalytic performance compared with particle photocatalyst. In a previous report, the phenomena that $NaNbO_3$ nanowires showed the best photocatalytic activity for hydrogen generation among several morphologies photocatalysts was possibly ascribe to its good crystallinity, large surface-to-volume ratio (S/V) and anisotropic aspect [19]. In the present case for CO_2 reduction, nanowires photocatalyst also showed higher activity. It is implied the good crystallinity, large surface-to-volume ratio (S/V) and anisotropic aspect are helpful to improve the photocatalytic activity for CO_2 reduction. All these suggest some useful information to develop the photocatalyst for CO_2 reduction and enhance efficiency of a photocatalytic material.

4 Conclusion

In this study, $NaNbO_3$ had been successfully developed as a photocatalyst for CO_2 reduction. The DFT calculations revealed that the top of VB consisted of O 2p orbital, while the bottom of CB was constructed by Nb 3d orbital, respectively. A band structure calculation showed the charge carrier in the CB was highly mobile. Compared with bulk $NaNbO_3$ samples, $NaNbO_3$ nanowires exhibited a much higher photocatalytic activity for CH_4 production. It was possibly due to crystallinity, surface-to-volume ratio and anisotropic aspect. In summary, the present research is positive, and is expected to supply some useful information for enhancing the performance of photocatalysts and developing a new serial of photocatalysts for CO_2 conversion.

Acknowledgments The authors would like to acknowledge financial support from the Fundamental Research Funds for the Central Universities JUSRP11010, as well as the National Basic Research Program of China 973 Program (Grant No. 2007CB613301).

References

1. Hiroshi Y, Tamura H (1979) Nature 282:817–818
2. Yin X, Moss JR (1999) Coord Chem Rev 181:27–59
3. Yang H, Lin H, Chien Y, Wu J, Wu HH (2009) Cata Lett 131:381–387
4. Roy SC, Varghese OK, Paulose M, Grimes CA (2010) Acs Nano 4:1259–1278
5. Koci K, Mateju K, Obalova L, Krejcikova S, Lacny Z, Placha D, Capek L, Hospodkova A, Solcova O (2010) Appl Cata B 96:239–244
6. Indrakanti VP, Kubicki JD, Schobert HH (2009) Energy Environ Sci 2:745–758
7. Wu JCS (2009) Catal Surv Asia 13:30–40
8. Teramura K, Okuoka S, Tsuneoka H, Shishido T, Tanaka T (2010) Appl Cata B 96:565–568
9. Ikeue K, Yamashita H, Anpo M, Takewaki T (2001) J Phys Chem B 105:8350–8355
10. Tseng IH, Chang WC, Wu JCS (2002) Appl Cata B 37:37–48
11. Dey GR, Belapurkar AD, Kishore K (2004) J Photochem Photobio A 163:503–508
12. Varghese OK, Paulose M, LaTempa TJ, Grimes CA (2009) Nano Lett 9:731–737
13. Yoong LS, Chong FK, Dutta BK (2009) Energy 34:1652–1661
14. Koci K, Obalova L, Matejova L, Placha D, Lacny Z, Jirkovsky J, Solcova O (2009) Appl Cata B 89:494–502
15. Wang CJ, Thompson RL, Baltrus J, Matranga C (2010) J Phys Chem Lett 1:48–53
16. Matsumoto Y, Obata M, Hombo J (1994) J Phys Chem 98: 2950–2951
17. Pan PW, Chen YW (2007) Cata Commun 8:1546–1549

18. Liu Y, Huang B, Dai Y, Zhang X, Qin X, Jiang M, Whangbo MH (2009) Cata Commun 11:210–213
19. Shi HF, Li X, Wang D, Yuan Y, Zou Z, Ye J (2009) Cata Lett 132:205–212
20. Hoffmann MR, Martin ST, Choi WY, Bahnemann DW (1995) Chem Rev 95:69
21. Linsebigler AL, Lu G, Yates JT (1995) Chem Rev 95:735
22. Shi HF, Li XK, Iwai H, Zou ZG, Ye JH (2009) J Phys Chem Solids 70:931–935
23. Segall MD, Lindan PJD, Probert MJ, Pickard CJ, Hasnip PJ, Clark SJ, Payne MC (2002) J Phys: Condens Matter 14:2717